Composites Part B 172 (2019) 679–689

Contents lists available at ScienceDirect

Composites Part B

journal homepage: www.elsevier.com/locate/compositesb

A multiscale micromechanical model of adhesive interphase between cement paste and epoxy supported by nanomechanical evidence

Jovan Tatar [a,*], Curtis R. Taylor [b], H.R. Hamilton [c]

[a] University of Delaware, Department of Civil and Environmental Engineering, 301 DuPont Hall, Newark, DE, 19716, USA
[b] University of Florida, Department of Mechanical and Aerospace Engineering, 312 Weil Hall, Gainesville, FL, 32611, USA
[c] University of Florida, Department of Civil and Coastal Engineering, 365 Weil Hall, Gainesville, FL, 32611, USA

ARTICLE INFO

Keywords:
Cement paste
Concrete
Epoxy
Adhesion
Interfaces
Interphase
Nanoindentation
Micromechanics

ABSTRACT

Even though epoxy adhesives are used extensively in concrete structures, little fundamental research has been conducted regarding bond formation mechanisms between the adhesive and concrete substrate, which obscures our understanding of degradation mechanisms in the bonded joints. When epoxy adhesive is applied to the concrete substrate, a transition region – termed interphase – is formed between the bulk epoxy and bulk cement paste/aggregate. Properties of interphase are thought to govern the macroscale behavior and durability of epoxy-concrete bonded systems. This work proposes an elastic multiscale model of the interphase region that is based on the existing body of knowledge on the topic. Site-specific statistical nanoindentation was used to experimentally evaluate the interphase region and verify the micromechanical model. Test results indicate that mechanical properties of the interphase region are different from those of bulk epoxy and cement paste. Experimental findings agreed with the postulated multiscale interphase model.

1. Introduction

Epoxy adhesives are extensively used in concrete infrastructures [1,2]. In these applications, adhesive bonds are exposed to a variety of harsh conditions that ultimately lead to a reduction of the load-carrying capacity of the adhesive joints. To design more durable adhesive joints, it is essential to understand the underlying mechanisms governing bond formation.

The adhesive bond between epoxy adhesive and concrete is a phenomenon that transcends multiple length scales. The conceptual bond formation model is presented in Fig. 1 for an example adhesive joint between externally bonded fiber-reinforced polymer (FRP) sheet and concrete, a common application for adhesives in concrete infrastructure.

At the macro scale, three distinct phases are observed in the bonded system: FRP, epoxy adhesive, and the concrete substrate. The bond between FRP and concrete is formed by means of epoxy adhesive that transfers load between the composite and substrate. Mechanical interlock is established primarily at micro-macroscale by the flow of epoxy into the holes, crevices, and pores of the concrete substrate. After it cures, epoxy locks in mechanically to the surface. At nano-microscale, the main bond-forming mechanisms are interphase formation [3] and hydrogen bonding between the adhesive joint constituents [4,5]. Interphase represents a transition region between the properties of neat epoxy adhesive and those of the substrate (concrete/cement paste), and it is thought to be formed by permeation and chemisorption of adhesive into the substrate. No work in the available literature has focused on the mechanical properties on the interphase, even though the interphase can govern the strength, crack growth characteristics, and durability of adhesive joints [6,7].

In this study, we propose an elastic multiscale interphase model for epoxy-cement paste adhesive interphase. Site-specific statistical nanoindentation characterization of the interphase region was performed to provide experimental evidence in support of the postulated model.

2. Multiscale interphase model

Motivated by the elastic multiscale model of cement paste developed by Ulm et al. [8] and informed by the review of literature and previous work done by the authors of this article [3,9], a model of epoxy-cement paste interphase was proposed. Multiple length scales were identified to capture the multiscale nature of the interphase: atomic scale, Level '0', Level I and Level II.

* Corresponding author.
E-mail addresses: jtatar@udel.edu (J. Tatar), curtis.taylor@ufl.edu (C.R. Taylor), hrh@ce.ufl.edu (H.R. Hamilton).

https://doi.org/10.1016/j.compositesb.2019.05.038
Received 17 December 2018; Received in revised form 21 March 2019; Accepted 5 May 2019
Available online 7 May 2019
1359-8368/

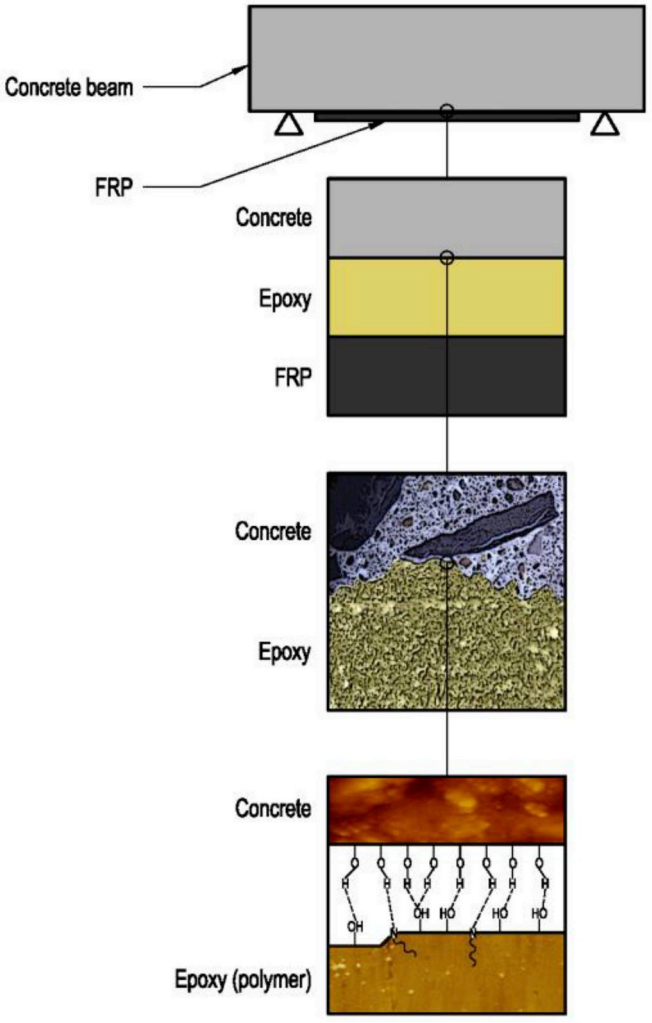

Fig. 1. Conceptual multiscale epoxy-concrete adhesive bond model.

2.1. Atomic scale

At the atomic scale, the exact stoichiometry of the main hydration product of cement paste, calcium silicate hydrate (C–S–H), is still an unknown. It has been confirmed, however, that the properties and structure of C–S–H are strongly affected by the mass ratio of Ca to Si [10]. A model of C–S–H, allowing for realistic Ca/Si ratios, was proposed by Pellenq et al. [11]. In its basal configuration (Ca/Si = 1), the model resembles a tobomorite with an interlayer space of 11 Å with two CaO layers and eight silicate chains. The interlayer Ca^{2+} ions balance out the negative charge of the configuration. To obtain a more realistic structure of C–S–H, in agreement with spectroscopic analyses results, neutral SiO_2 groups of silica tetrahedral were removed. This process resulted in "defective" C–S–H structures allowing to represent a range of realistic Ca/Si ratios. Utilizing this model [12], a combinatorial study was conducted to determine the relationship between the C–S–H structure (defined by Ca/Si ratio) and the elastic modulus. The authors found that elastic modulus is inversely proportional to increasing Ca/Si ratio—high Ca/Si ratios result in C–S–H structure with more defects.

The epoxy molecule is characterized by the presence of epoxide groups that can be polymerized with a curing agent, commonly referred to as *hardener*. The most typical epoxy molecule in construction adhesives is diglycidyl ether of bisphenol A (DGEBA). A common class of curing agents are amines, characterized with reactive amine groups. DGEBA epoxide groups react with curing agent through nucleophilic addition – this reaction results in formation of permanent chemical bonds (cross-links) between the epoxy and the curing agent. As the curing reaction progresses, a highly cross-linked polymer network is formed. The density of the cross-linked network defines the mechanical and thermal properties of epoxy. Due to the permanent nature of cross-links, epoxy is a thermosetting polymer: when heated up above the glass transition temperature (T_g), epoxy softens but does not melt.

2.2. Level '0'

Level '0' represents the length scale where the separation between the atomic and continuum phenomena occurs. In neat cement paste, Level '0' is characterized by formation of C–S–H solid (Fig. 2) by hydration of C_3S and C_2S. The C–S–H solid was found to have an approximate size of 5.6 nm (Fig. 2) [13]. Many studies focused on investigations at Level '0', [14–16]. A mutual agreement is that C–S–H solid has colloid properties. According to Jennings [16], the structure of C–S–H at Level '0' can be regarded as a collection of globular structures with intra-globular nanoporosity of approximately 18%. Structure of the "basic building blocks" of C–S–H globules is assumed to be layered. The spaces between the "basic building blocks" represent nanoporosity, which carries structural water.

When C–S–H contacts with epoxy, aminated hardener can generate a localized increase in pH, which results in partial ionization of silanol sites in C–S–H structure, causing dissolution of C–S–H solid [17]. As explained by Djouani et al. [17]—in relatively low pH—the C–S–H is charged negatively due to the silanol sites supported by the silicon tetrahedra (Fig. 3a). At higher pH, the negative charge is carried by the non-bridged silicate tetrahedra: the Ca^{2+} ions balance out this negative charge. The consequence of adsorption of hardener by the C–S–H is, thus, a higher Ca/Si ratio of C–S–H crystals as confirmed by chemical analyses. The shift from low to high Ca/Si ratios results in transition of C–S–H structure from layered to a more amorphous arrangement (Fig. 4), which was shown (both experimentally and through atomistic simulations) to result in a decrease of reduced (indentation) modulus of

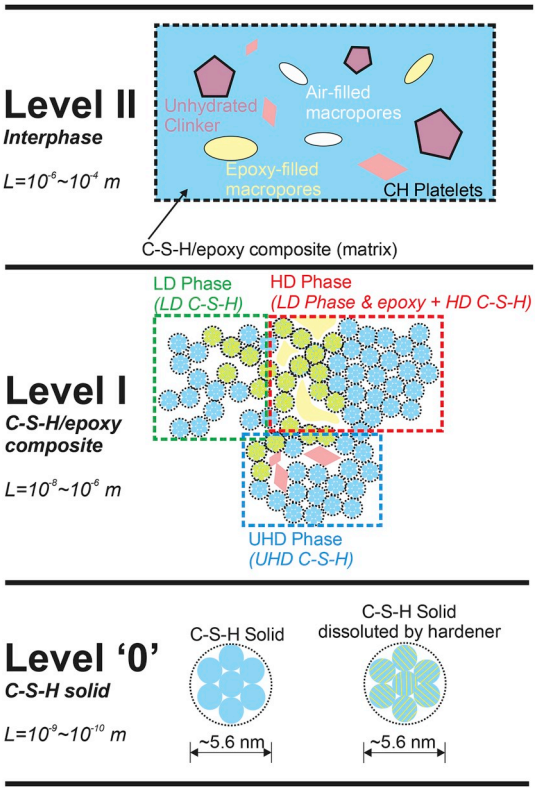

Fig. 2. Postulated multiscale model of cement paste interphase.

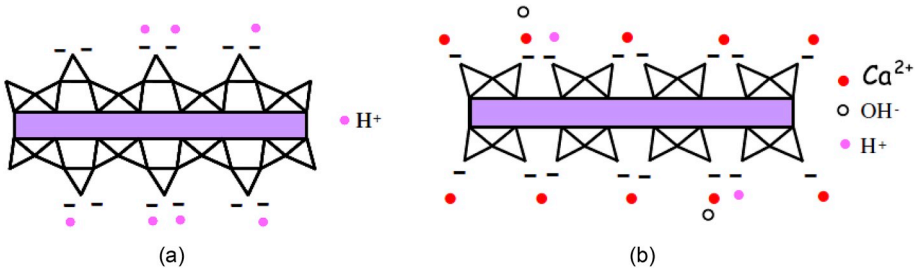

Fig. 3. Structure of C–S–H at proposed by Viallis-Terrisse [18], as cited in Djouani et al. [17].: (a) pH = 10 (corresponding to Ca/Si ratio of 0.66); and (b) pH = 12.5 (corresponding to Ca/Si ratio of 1.5). "Interactions of fully formulated epoxy with model cement hydrates", [17]; reprinted with permission from the publisher (Taylor & Francis Ltd, http://www.tandfonline.com).

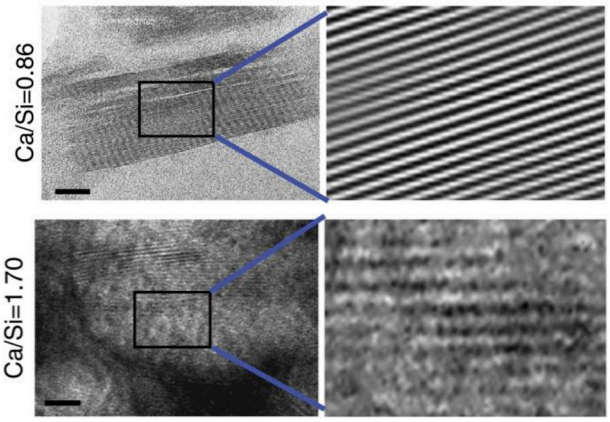

Fig. 4. Tunneling Electron Microscopy (TEM) image of C–S–H structure at Ca/Si ratio of 0.86 (top) and 1.7 (bottom). Reprinted by permission from Macmillan Publishers Ltd: NATURE COMMUNICATIONS (Qomi, M. J. A., Krakowiak, K. J., Bauchy, M., Stewart, K. L., Shahsavari, R., Jagannathan, D., Brommer, D. B., Baronnet, A., Buehler, M. J., Yip, S., Ulm, F. J., Van Vliet, K. J., Pellenq, R. J. M. "Combinatorial molecular optimization of cement hydrates"), copyright (2014).

C–S–H [12,19] – indicating degradation in mechanical properties. Additionally, ettringite, which is intrinsically a component of C–S–H structure was found to be similarly affected by the amine-rich hardener. The dissoluting effect of amine hardener is also well-pronounced in isolated calcium hydroxide (CH) crystals [17].

2.3. Level I

At Level I, gel porosity defines the properties of the C–S–H matrix. Depending on the porosity, two structurally distinct types of C–S–H exist: (1) a more porous, low-density C–S–H (LD C–S–H); and (2) a relatively more densely packed, high-density C–S–H (HD C–S–H) [20]. also demonstrated that a nanocomposite of calcium hydroxide (CH) and C–S–H exists at Level I, commonly referred to as ultra-high-density C–S–H (UHD C–S–H). Hydrated aluminates, ettringite, and monosulfate, intrinsically occur within the C–S–H matrix. Gel porosity is on the length order of magnitude of about 5 nm and can contain non-structural water, and therefore contributes to the mass transport properties of cement paste. Characteristic length scale of Level I is in the range 0.1–1 μm.

When penetrated by an epoxy adhesive, the properties of C–S–H can change due to their interaction with epoxy hardener. Per Tatar et al. [3]; low-viscosity epoxy can occupy larger accessible pores by permeation and capillary suction which is expected to further modify the mechanical properties of LD C–S–H. Even though HD and UHD C–S–H gel pore space would likely not be accessible to DGEBA macromolecules, presence of dissolved C–S–H solid is still possible within HD C–S–H and UHD C–S–H due to strong preferential attraction between the aminated hardener and C–S–H [4].

Chemo-morphological changes in C–S–H phases caused by epoxy are characterized by our model (Fig. 2). At Level I, cement paste interphase is postulated to contain:

1. LD Phase consisting of (i) C–S–H solid, (ii) dissoluted C–S–H solid, and (iii) porosity that is inaccessible to the crosslinked network of epoxy;
2. HD Phase consisting of (i) nanocomposite of LD Phase and epoxy, (ii) densely packed C–S–H solid that is inaccessible to epoxy crosslinked network, and (iii) dissoluted C–S–H solid); and
3. UHD Phase consisting of (i) nanocomposite of densely packed C–S–H solid and dissoluted C–S–H solid, (ii) and CH crystals.

2.4. Level II

At a range of length scales from 1 to 100 μm, interphase can be considered a composite (Fig. 2) consisting of: (i) C–S–H/epoxy composite matrix with unhydrated cement clinker (C_3S, C_2S, C_3A, C_4AF) inclusions; (ii) macroporosity (filled with epoxy and/or air); and (iii) large CH crystals with a characteristic size on the order of 1 μm, representing inclusions. Transport phenomena at this length scale are governed primarily by a network of capillary pores, which is a result of excess mixing water in the neat cement paste (w/c ratio). Distribution and connectivity of capillary pores are deemed to govern the accessibility of smaller gel pores to the curing epoxy adhesive [3].

2.5. Continuum mechanics relationship between Level '0' through level II in cement paste

Currently available experimental techniques (nanoindentation) allow access to material properties (elastic modulus and hardness) found at Level I. Works of multiple researchers have concentrated on micromechanical modeling of cement paste at Level I in an attempt to establish a relationship between nanoindentation measurements and macroscopic/effective material properties [21–24]. By assuming that each nanoindentation experiment represents a single phase in the cement paste with spherical geometry, multiple studies [22,24] successfully computed effective elastic modulus of cement paste that matched the macroscopic elastic modulus obtained by other measurement methods (ultrasonic pulse velocity, and instrumented microindentation). Both studies assumed a *virtual* N-phase composite with spherical morphology where N is the total number of indentation experiments, and therefore, each indentation experiment represents a single phase in the composite; effective elastic properties of the virtual composite were determined based on the self-consistent continuum micromechanics model.

The goal of the above-described approach was upscaling of elastic properties obtained from nanoindatation—elastic moduli corresponding to length scale of Level I were used to compute effective properties of

Level II [25]. employed a reverse approach—from nanoindentation data corresponding to LD and HD C–S–H (Level I), with aid of continuum micromechanics, they back-calculated the elastic properties of C–S–H solid (Level '0'). The procedure was based on Jenning's model of C–S–H [16]) that represent LD and HD C–S–H by loosely and densely packed granules, respectively. By assuming spherical morphology of C–S–H, the researchers used polycrystalline self-consistent micromechanical model formulation to extrapolate the packing density of each of the phases and determine the elastic modulus of C–S–H building blocks from nanoindentation data. Packing density of C–S–H was defined as:

$$\eta = \frac{V_s}{V_t} \tag{1}$$

where V_s is the volume of C–S–H solid within the representative elementary volume (REV), V_t.

Results of the employed analytical procedure were in good agreement with independently experimentally obtained packing densities of LD and HD C–S–H of 0.63 and 0.76 [16], respectively. The method also provided an estimate of reduced modulus of a single globule (C–S–H solid—Level '0') of approximately 65 GPa. To date, no direct measurements of the elastic properties of C–S–H solid have been reported. This is mainly due to the inability of available nanomechanical characterization instrumentation to access the length scale of C–S–H solid. The elastic properties of C–S–H solid, however, have been quantified via atomistic simulations [11]; the obtained reduced modulus from a computational atomistic model of C–S–H (66–68 GPa) compared well with that extrapolated from nanoindentation data (65 GPa).

In the work of Constantinides and Ulm [25], it was shown that Mori-Tanaka homogenization scheme cannot accurately model the relationship between C–S–H packing density and modulus; this is mainly because an underlying assumption in the Mori-Tanaka method is that C–S–H solid is the matrix phase while the porosity represents spherical inhomogeneities within the C–S–H matrix, which is a fundamentally incorrect representation of the C–S–H morphology. Inability of Mori-Tanaka to provide correct estimates of C–S–H solid elastic modulus further backs up the assumption of nanogranular morphology of C–S–H solid, with no distinct matrix phase: the stress is transferred through contact interaction between the C–S–H globules.

3. Experimental verification of multiscale continuum mechanics model of adhesive interphase

To verify the proposed elastic multiscale model of the interphase between epoxy and cement paste, nanoindentation experiments were conducted in the interphase region. Existence of interphase was previously confirmed via Raman spectroscopy [3]. Using the proposed elastic multiscale model of interphase (Fig. 2) nanoindentation results were correlated with the postulated interphase model.

3.1. Materials and methods

Nanoindentation was used to evaluate the nanomechanical properties of the interphase. All nanoindentation experiments were conducted using an Asylum Research MFP NanoIndenter™ (Oxford Instruments, Santa Barbara, CA). The equipment utilizes the optical lever system of the MFP-3D atomic force microscope, combined with a vertical nanoindentation probe. The gold-coated silicon chip on the back of the nanoindentation fixture reflects the laser light back through a collimating lens to a mirror that sends it to a photodetector. Depending on the position of the laser light relative to the four quadrants of the photodetector, the lateral and vertical deflection of the indenter tip are determined. Displacement of the indenter probe is piezo driven with closed-loop feedback via linear voltage displacement transducer sensors. Given the vertical setup of the nanoindentation system, the lateral component is negligible. The instrument has a displacement resolution of 0.3 nm and load resolution of 75 nN. Tip area calibration and all load-displacement curves were analyzed for hardness and reduced modulus per the Oliver and Pharr method, which is described elsewhere [26].

3.1.1. Analysis of indentation data via Gaussian mixtures model

The purpose of nanoindentation experiments in cementitious materials is to provide access to the individual mechanical properties of the constituent material phases within the cement paste. Indentation elastic properties (reduced modulus and hardness) will primarily depend on the size and depth of the indent, which dictates the length scale of testing. Given the multiscale nature of cement paste, it is, therefore, necessary to define the range of indentation interaction volumes that will allow access to the specific length scales. Length scale on the order of magnitude between 0.1 and 1 μm is, presently, the smallest material length scale of cement paste that is accessible for nanomechanical characterization by nanoindentation; thus, nanoindentation can provide access to mechanical properties of low-density calcium silicate hydrate (LD C–S–H), high-density calcium silicate hydrate (HD C–S–H), ultra-high-density calcium silicate hydrate (UHD C–S–H) and unhydrated clinker grains.

The radius of nanoindentation interaction volume in cement paste was found to be about 3–4 times the maximum indentation depth [21], meaning that the indentation load should be selected so that the maximum indentation depth does not exceed 500 nm. Higher loads result in larger interaction volumes and provide "homogenized" (bulk) response of the material containing nanomechanical information of multiple material phases. Load that allows for adequate indentation depths is 2 mN.

Due to the heterogeneity of the cement paste, nanoindentation experiments are generally conducted in a grid of minimum 300 indents [25]). Collected nanoindentation data is, thus, inherently a multivariate distribution representing a mixture of mechanical properties corresponding to different material phases found in the indented area on the sample. Following the assumption that mechanical properties of the material constituents are each normally distributed, the mechanical properties of individual constituents can be determined by fitting a number of Gaussian distributions to the experimental distribution of data. In that case , the number of fitted Gaussian distributions corresponds to the number of material phases with distinct mechanical properties [27].

To determine the number of distinct material phases (Gaussian distributions), based on the contrast between the measured material properties, Bayesian Information Criterion (BIC) can be employed [27]. BIC [28] evaluates the goodness-of-fit for a multimodal Gaussian distribution by introducing a penalty score for overfitting (excessive number of Gaussian distributions). Minimum BIC score corresponds to the optimal number of Gaussian distributions existing within a multimodal distribution.

A specific number of Gaussian distributions based on the BIC results can then be fitted to the experimental distribution of nanoindentation data by utilizing a Gaussian mixture model. The method reveals indentation properties associated with each of the identified material phases with distinct mechanical properties and allows their relative volume fractions to be determined. The iterative procedure fits the desired number of Gaussian distributions to multivariate data, using maximum likelihood via the expectation maximization algorithm. Krakowiak et al. [27] demonstrated that the number of distinct material phases determined from nanoindentation data by analytical means, through BIC, exhibited a satisfying correlation with independent chemical analyses conducted via energy dispersive spectroscopy (EDS). Deconvolution of mechanical data did not, however, differentiate between CSH and hydrated aluminates (AFt and AFm) which are an intrinsic component of C–S–H matrix. Additionally, spectroscopic analyses revealed the presence of C_4AF crystals within the CH-dominated family.

3.1.2. Materials

For this study, epoxy-cement paste bonded specimens were made. The cement paste samples with w/c ratio of 0.40 were prepared by mixing in a high shear mixer; Type I/II Portland cement was used. High shear mixing was chosen over traditional paddle mixing to produce a more uniform mixture. This mixing method is deemed to break down the agglomerations of cement clinker during mixing and provide optimal wetting of the cement powder, which results in a more homogeneous mixture when compared to traditional mixing methods. Cement paste samples were cast in brass molds to make 5-cm cubes. Following the initial cure, after 24 h, cement paste samples were placed in a lime solution for 6 months and air-dried for a minimum of 3 months prior to sample preparation.

Samples were then cut in a slow-speed diamond saw (Allied TechCut 4) into 1 cm cubes. The bonding surfaces on each of the cubes were flattened with a 240 grit silicon carbide polishing disc. Polishing was then performed in multiple steps with silicon carbide polishing paper and finished with a 1 μm diamond suspension in polyethylene glycol (PEG) on a silk cloth. Polished surfaces were cleaned with acetone between the polishing steps. Acetone was chosen for cleaning of cement paste as it was previously shown that it does not affect the properties of C–S–H [29]. The polishing procedure resulted in smooth appearance without a glossy finish with a root mean square surface roughness (R_{RMS}) on the order of 300–400 nm on a 50 × 50 μm area, as measured on Asylum Research MFP-3D atomic force microscope (AFM). Lack of glossy finish was believed to be important to alleviate the effects of extremely low surface tortuosity on reduction in surface free energy, which could affect the wetting ability of the adhesive.

Two cement paste cubes were placed approximately 2–3 mm apart and wrapped with a PTFE tape. Epoxy adhesive consisting of diglycidyl ether of bisphenol A (DGEBA, Hexion® EPON 826) resin with epoxide equivalent weight of 178–186 g/eq, and poly(oxypropylene) diamine (POPDA, Hunstman ® Jeffamine D-230) hardener with an average molecular weight of 230 g/mol was mixed in a weight ratio of 100:32.9, which corresponds to stoichiometric equivalence between the functional groups. The initial viscosity of the mixture is approximately 9 cps, per [30]. Chemical structures of DGEBA and POPDA are shown in Fig. 5. Vigorously mixed epoxy was slowly injected into the gap between the cement paste cubes with a syringe. The bonded samples were cured for 7 days, before proceeding with polishing of the top surface intended for characterization.

Multiple polishing procedures were explored. However, it was found that successive polishing with silicon carbide sandpaper in the following order 320, 600, 800, 1200, 4000, followed by 2–3 min on 1 μm diamond solution in PEG on Buehler TexMet P polishing pad created the smoothest surface in terms of R_{RMS}.

Polishing on each of the silicon carbide grits was done until the scratch marks from the previous grit were imperceptible under the optical microscope. Diamond solution polishing did not appear to reduce the surface roughness following 4000 carbide grit polishing, however, it was performed for a short period of time to remove sporadic scratches on the sample surface from 4000 grit polishing. Samples were cleaned with 99% isopropanol between the polishing steps. Isopropanol was chosen over more potent solvents to avoid possible degradation of epoxy cross-link network and C–S–H [29]. The final polished surface had a mirror finish (Fig. 6) with R_{RMS} in 200–300 nm range on 50 × 50 μm area. The measured surface roughness was well within the range of the lower bound of intrinsic surface roughness of cement paste determined by Trtik et al. [31]. Any decrease in roughness beyond that limit is believed to be due to polishing artifacts and surface damage.

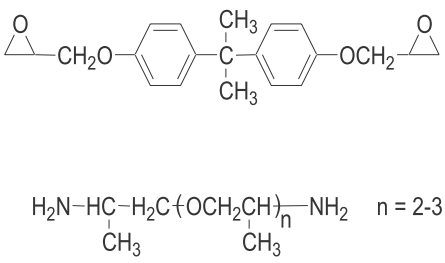

Fig. 5. Chemical structures of epoxy adhesive components: (a) DGEBA; and (b) POPDA.

3.1.3. Experimental procedures

Nanoindentation experiments were conducted in the interphase region of the epoxy-cement paste specimen (Fig. 6). All indentations were performed at room temperature (~23 °C) with a maximum load of 2 mN. Indents were made with a diamond Berkovich tip (nominal tip radius ~ 90 nm) with the loading function defined as loading, hold, and unloading times of 5 s, 3 s, 5 s, respectively. Load-controlled indentations resulted in maximum indentation depths between approximately 200-300 nm.

Site-specific nanoindentation experiments were performed in 5 parallel lines along the interface; each indentation area was 90 × 90 μm and contained a total of 50 indents (Fig. 7). To obtain a substantially large dataset for statistical analysis, the experiment was repeated on 30 areas, to generate a total of 300 indents per each line parallel to the interface. The reference line of indents was located approximately 12.5 μm from the interface within the bulk epoxy; the spacing between the lines of indents was 22.50 μm. Location of the interface was determined using the imaging mode of the indenter at each indentation location. Control data consisting of 300 indents was collected far from the interface, in bulk cement paste.

3.2. Results and discussion

3.2.1. Data analysis

Sample nanoindentation load-displacement curves for epoxy, C–S–H, and cement clinker are shown in Fig. 8. A significant difference in the slope of unloading portion (stiffness) between the curves is apparent, resulting from dissimilarity in stiffness between the corresponding material phases.

Gaussian mixtures deconvolution algorithm was utilized to identify clusters of data with distinct mechanical properties within the experimental data (Fig. 9). The process was completely automated through a Matlab function. The validity of the approach was verified on an artificially generated multivariate distribution with multiple Gaussian distribution component of known parameters. An example of clustered indentation data corresponding to one of the indentation lines within

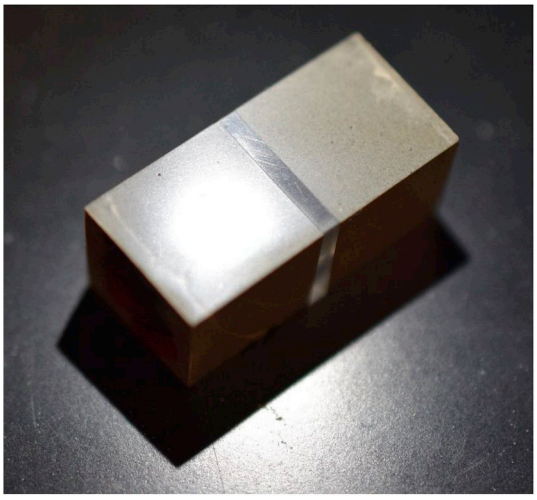

Fig. 6. Light reflecting from the surface of cement paste-epoxy sandwich sample.

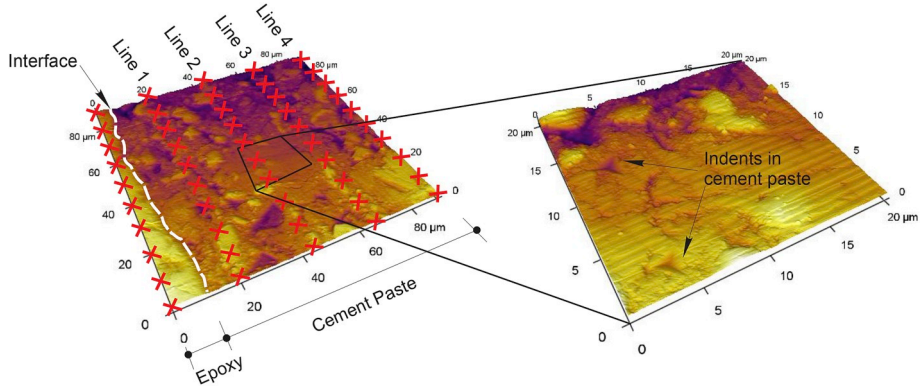

Fig. 7. Locations of indents relative to the interface shown in AFM images.

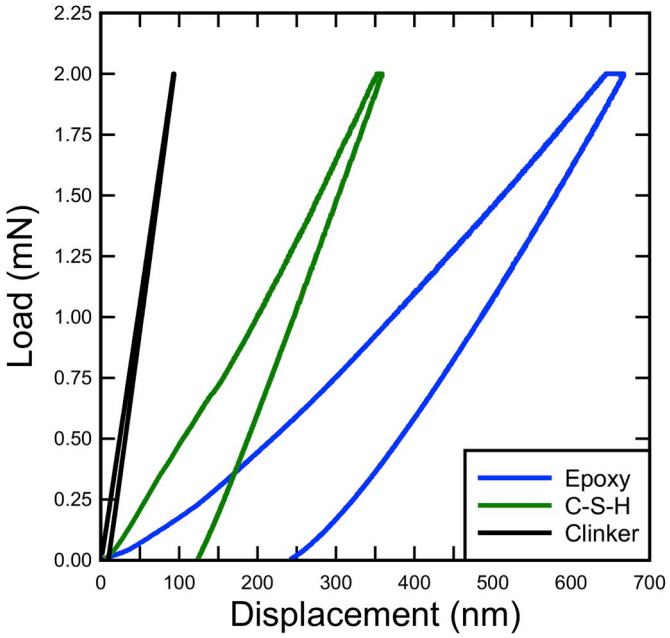

Fig. 8. Example load vs. displacement plots for epoxy, C–S–H and clinker.

the interphase is graphically shown in Fig. 9a, for four material phases (as determined by BIC). Example of deconvoluted reduced moduli data of the portion of data dominated by cement hydrates (E_r<65 GPa) is shown in Fig. 9b as a probability density function.

The deconvolution algorithm was applied to each line of indents in the cement paste sample as well as to a control location that was located far away from the interface. Results of the deconvolution procedure for reduced modulus (E_r) and hardness (H) at the control location are summarized in Table 1. Graphical representation of clustered nanoindentation data, and reduced moduli data in a form of probability density function (PDF) are given in Fig. 9a and b, respectively. The four identified material phases at control location correspond to LD C–S–H, HD C–S–H, UHD C–S–H, and unhydrated clinker grains based on the available literature (Table 2).

As discussed in the literature review section, morphologically, LD C–S–H can be considered an equivalent of randomly packed spheres (C–S–H globules), while the HD C–S–H is an equivalent of more orderly packing of spheres [21]. UHD C–S–H was found to be a nanocomposite of HD C–S–H and calcium hydroxide (CH) present in the gel pores of C–S–H [20]. 'Clinker' phase is mostly composed of unhydrated clinker grains [23] Given that unhydrated cement particles are large solid crystals with no porosity, they are not thought to contribute significantly to transport of epoxy in cement paste. The focus of the later discussions will be primarily on the most porous phases—LD C–S–H and HD C–S–H. The data is very scattered for clinker phase due to the varying size of clinker crystals. If the crystal size is smaller than the indentation interaction volume, then the response will contain composite mechanical properties of the crystal and surrounding material. UHD C–S–H also has

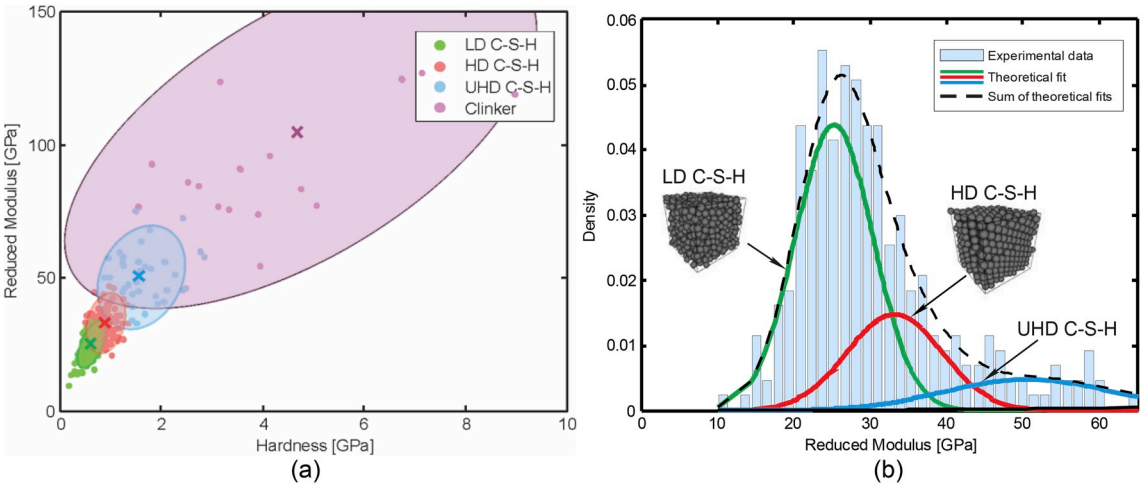

Fig. 9. Nanoindentation test results for control location: (a) Gaussian mixtures deconvolution of reduced modulus and hardness data represented by cluster allocation; (b) deconvoluted reduced modulus data for a range of reduced moduli corresponding to cement hydrates (<65 GPa).

Table 1
Summary of nanoindentation mechanical properties at control location (far away from interface).

Property	LD C–S–H		HD C–S–H		UHD C–S–H		Clinker	
	f_k	$\mu_k \pm \sigma_k$[GPa]	f_k	$\mu_k \pm \sigma_k$[GPa]	f_k	$\mu_k \pm \sigma_k$[GPa]	f_k	$\mu_k \pm \sigma_k$[GPa]
E_r	0.56	25.3 ± 5.1	0.23	33.2 ± 6.2	0.13	50.7 ± 10.8	0.08	104.6 ± 37.7
H	0.56	0.60 ± 0.15	0.23	0.88 ± 0.21	0.13	1.57 ± 0.51	0.08	4.69 ± 2.61

Table 2
Ranges of indentation mechanical properties for the three C–S–H phases based on analysis of large population of different OPC samples by Vandamme [32], as cited in Vanzo [33].

Material phase	Mean reduced modulus [GPa]	Mean hardness [GPa]	Mean packing density
LD C–S–H	16–26	0.27–0.88	0.62–0.71
HD C–S–H	27–40	0.74–1.45	0.69–0.81
UHD C–S–H	36–54	1.15–2.35	0.78–0.90

a significant scatter in data due to the varying size of CH crystals within its structure in addition to the possible occurrence of C_4AF crystals within the interaction volume. LD and HD C–S–H have a relatively low variation in mechanical properties which is mostly due to them occupying the majority of the material volume.

The naming of four phases in the interphase region was adjusted to reflect the fact that this region was modified by the presence of epoxy, per Fig. 2. Consequently, the phases were named: 'LD Phase', 'HD Phase', 'UHD Phase', and unhydrated 'clinker'. Summary of Gaussian mixtures deconvolution on interphase data is presented in Table 3 and Table 4. Example of nanoindentation data and Gaussian mixtures deconvolution results from nanoindentation 'Line 2' (Fig. 7) are graphically presented in Fig. 10.

Reduced modulus of bulk epoxy was determined to be 4.40 GPa with a standard deviation of 0.39 (COV = 0.09), from a population of 100 indents. Measured reduced modulus corresponds to an elastic modulus of 3.70 GPa (assuming Poisson's ratio of 0.4, per [34]), which compares well to the value determined from tensile tests on 165 mm long coupons (Type I coupon—ASTM D638 [35]) of 3.45 GPa [30]. The average hardness of epoxy was 0.18 GPa with a standard deviation of 0.02 (COV = 0.12).

3.2.2. Nanomechanical properties of interphase constituents

Fig. 11 shows the spatial variation of average values of reduced moduli and hardness for LD Phase and HD Phase. Hardness measurements show similar trends (Table 4). Lower reduced moduli of LD and HD Phase near the interface are a result of their chemical reaction with the epoxy hardener (POPDA).

Effect of dissolution of hydrates due to their interaction with epoxy on their nanomechanical properties, according to herein presented experimental results, are most emphasized close to the interface. By distancing from the interface, the effect dissipates, which results in the stiffening effect of epoxy matrix on the measured moduli of the LD and HD C–S–H phases. HD Phase (corresponding to HD C–S–H in neat cement paste), particularly, has higher values of reduced modulus at 55 μm and 77.5 μm away from the interface than the control, which suggests that the softening effect of epoxy hardener is likely dependent on the concentration of hardener. Spatial variations in nanomechanical properties of UHD Phase and Clinker were not studied due to the inherent variation in mechanical properties of the two material phases.

To determine the extent of influence of epoxy hardener on the nanomechanical properties of LD and HD C–S–H, a two-sample unpaired *t*-test statistical analysis was conducted. The goal of the analysis was to verify if a statistically significant difference in means exists between two groups of data that are being compared. Unpaired *t*-test was chosen because it does not assume equality of variance nor equal sample sizes. All tests were performed for a significance level of 0.05. Given the likelihood of exhibiting a rare event (Type I error) when conducting multiple comparisons, the Bonferroni correction was applied by dividing the desired significance level of 0.05 by the number of comparisons (10), yielding a significance level of 0.005. When the calculated P-value is greater than the set significance level, then the difference in means is not considered statistically significant.

The results of unpaired *t*-test for LD Phase reduced moduli are shown in Table 5. It appears that no statistically significant difference exists between means at 10 μm and 32.5 μm away from the interface, while both populations are significantly different from the control value. On the other hand, means at 55 μm and 77.5 μm away from the interface are considered statistically equal; both means are equal to the control value, too. For HD Phase (Table 6), again, no statistically significant difference between means at 10 μm and 32.5 μm away from the interface exist. However, only the mean at 77.5 μm from the interface is deemed statistically equal to that measured in a control set of indents.

Based on the analysis of data, there is a difference between means observed at 10 μm and 32.5 μm, and those observed at 55 μm and 77.5 μm away from the interface. The effects of hardener on the reduced modulus are likely dependent on the concentration of hardener which explains why the degradation of the reduced modulus of LD and HD C–S–H is more statistically significant closer to the interface (10 and 32.5 μm).

3.2.3. Volume fractions of interphase constituents

When considering chemo-morphology of material phases in the cement paste interphase, it should be noted that the structure of C–S–H would have been modified by the presence of epoxy. Thus, it was necessary to evaluate the change in volume fractions of different materials phases with distance from the interface. Volume fractions of each of the constituent phases were determined by dividing the area under each of the theoretical Gaussian fits by the area under "sum of theoretical fits", as graphically shown in Figs. 9b and 10b. Fig. 12 indicates a significant difference in the distribution of volume fractions with respect to distance from the interface. Particularly, the ratio of volume fraction of LD Phase to that of HD Phase is changing with the distance from the

Table 3
Summary of reduced moduli within interphase.

Location [um]	LD Phase		HD Phase		UHD Phase		Clinker	
	f_k	$\mu_k \pm \sigma_k$[GPa]	f_k	$\mu_k \pm \sigma_k$[GPa]	f_k	$\mu_k \pm \sigma_k$[GPa]	f_k	$\mu_k \pm \sigma_k$[GPa]
10	0.15	18.8 ± 3.1	0.59	29.4 ± 5.9	0.19	53.5 ± 19.0	0.07	80.2 ± 38.3
32.5	0.25	20.1 ± 4.1	0.43	30.2 ± 5.6	0.22	42.7 ± 8.5	0.10	97.0 ± 34.3
55	0.41	25.9 ± 5.4	0.39	37.6 ± 8.7	0.09	55.5 ± 10.1	0.10	112.7 ± 42.5
77.5	0.35	24.9 ± 5.4	0.44	34.9 ± 9.9	0.19	60.6 ± 15.4	0.03	140.5 ± 30.2

Table 4
Summary of hardness within interphase.

Location [um]	LD Phase		HD Phase		UHD Phase		Clinker	
	f_k	$\mu_k \pm \sigma_k$[GPa]	f_k	$\mu_k \pm \sigma_k$[GPa]	f_k	$\mu_k \pm \sigma_k$[GPa]	f_k	$\mu_k \pm \sigma_k$[GPa]
10	0.15	0.43 ± 0.13	0.59	0.66 ± 0.20	0.19	1.41 ± 0.62	0.07	4.29 ± 2.01
32.5	0.25	0.44 ± 0.11	0.43	0.73 ± 0.18	0.22	1.17 ± 0.42	0.10	4.44 ± 2.99
55	0.41	0.57 ± 0.15	0.39	0.92 ± 0.29	0.09	1.83 ± 0.74	0.10	5.07 ± 2.35
77.5	0.35	0.58 ± 0.15	0.44	0.86 ± 0.22	0.19	2.32 ± 1.06	0.03	6.05 ± 3.64

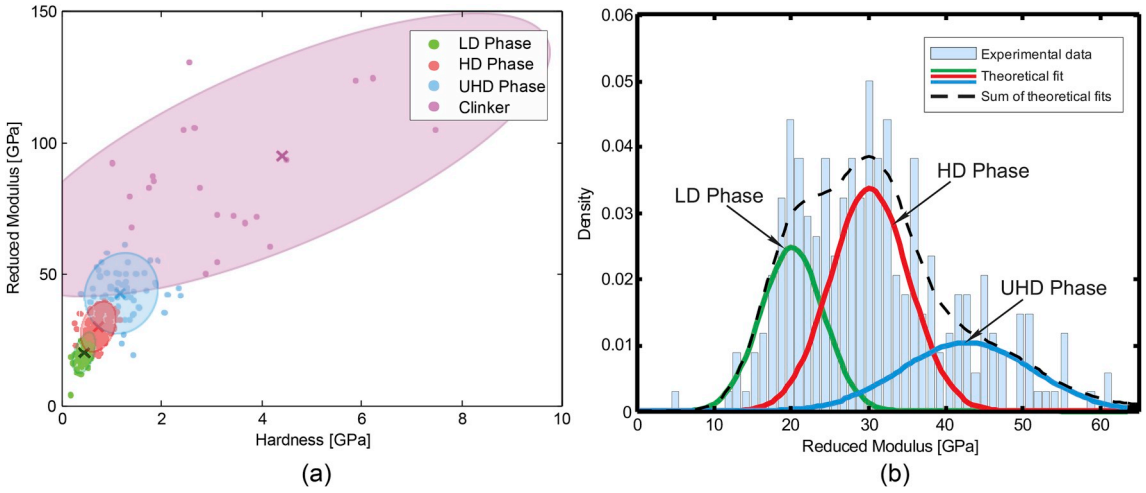

Fig. 10. Nanoindentation test results for interphase Line 2: (a) Gaussian mixtures deconvolution of reduced modulus and hardness data represented by cluster allocation; (b) deconvoluted reduced modulus data for a range of reduced moduli corresponding to cement hydrates (<65 GPa).

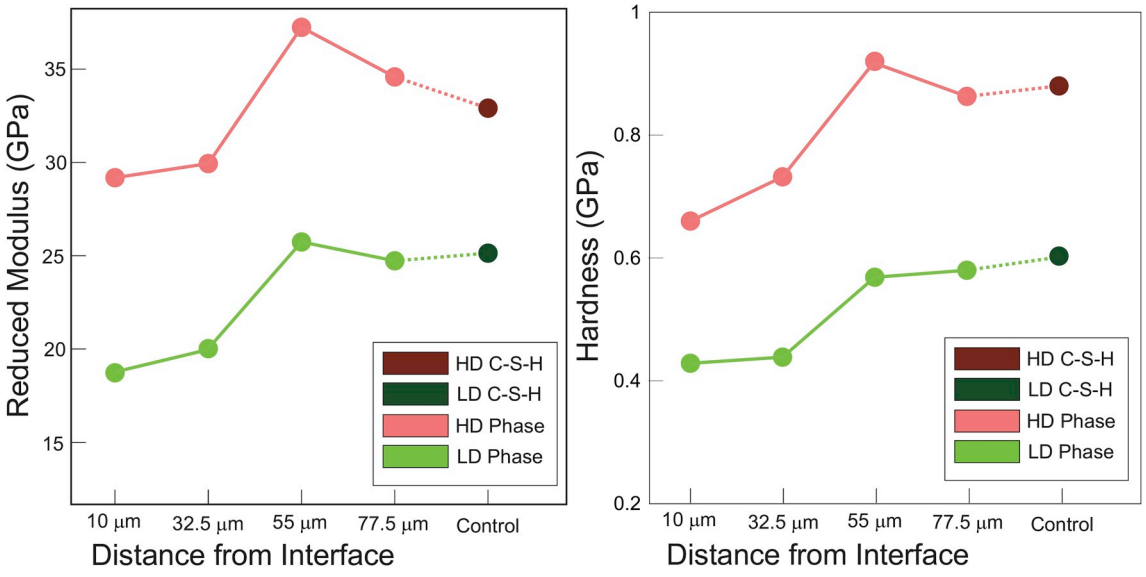

Fig. 11. Change in mean reduced modulus as a function of distance from interface.

Table 5
P-values for two-sample unpaired *t*-test on reduced moduli of LD Phase; bolded font signifies P > 0.005.

Distance from interface (μm)	10	32.5	55	77.5	Control
10	1	**0.069**	0.0001	0.0001	0.0001
32.5		1	0.0001	0.0001	0.0001
55			1	**0.165**	**0.334**
77.5				1	**0.538**
Control					1

Table 6
P-values for two-sample unpaired *t*-test on reduced moduli of HD Phase; bolded font signifies P > 0.005.

Distance from interface (μm)	10	32.5	55	77.5	Control
10	1	**0.232**	0.0001	0.0001	0.0001
32.5		1	0.0001	0.0001	0.0007
55			1	0.0231	0.0003
77.5				1	**0.194**
Control					1

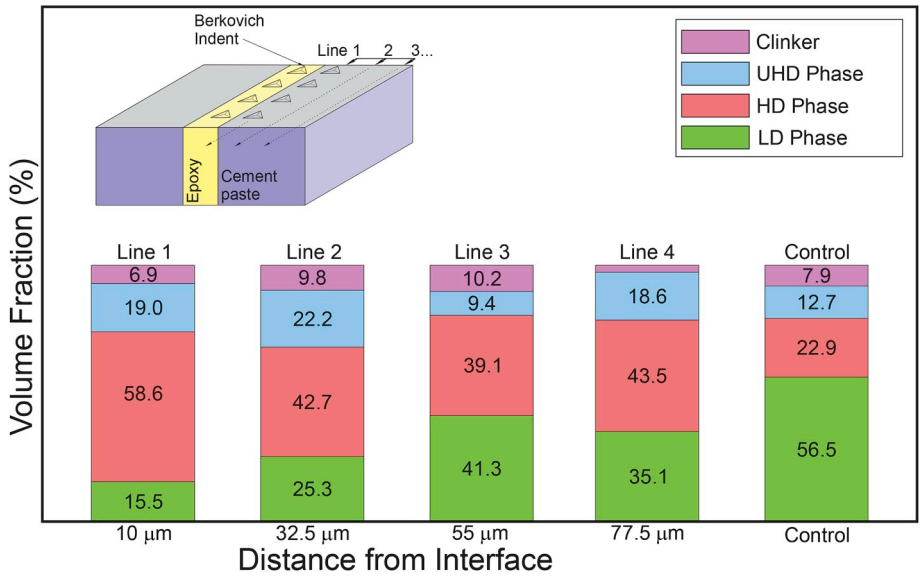

Fig. 12. Volume fractions of material phases as a function of distance from interface. Note that in "Control" group, material phases (top to bottom) correspond to LD C–S–H, HD C–S–H, UHD C–S–H and clinker.

interface: the volume fraction of LD Phase is increasing on the account of HD Phase. While there is some variation in volume fractions of UHD Phase and Clinker with respect to distance from interface, it is not possible to decipher how statistically significant these variations are due to the inherent scatter of data associated with the two materials phases.

Based on the experimental findings from Fig. 12, it is herein postulated that LD Phase corresponds to LD C–S–H that has not been accessible to the epoxy penetrating the cement paste matrix. This portion LD C–S–H was, however, involved in adsorption of epoxy hardener close to the interface which resulted in degraded reduced moduli of this phase (at 10 and 32.5 μm away from the interface). Therefore, as postulated by the model (Fig. 2) and demonstrated by the data —HD Phase represents a composite consisting of: (1) HD C–S–H; and (2) composite of LD C–S–H and epoxy. Existence of composite of HD C–S–H and epoxy is believed to be unlikely mainly due to the size of gel pores characteristic for HD C–S–H (which were found to be so small as to be inaccessible to nitrogen molecules by Jennings [16]). Based on the above-postulated modifications of cement paste microstructure in presence of epoxy, it can be deduced that the distribution of nanomechanical material properties of material phases (reduced moduli and hardness values) of cement paste-epoxy nanocomposite would be dissimilar from that of neat cement paste. The hypothesis that the ratio of volume fractions of LD Phase to that of HD Phase is due to the stiffening of LD C–S–H when saturated with epoxy is supported by continuum mechanics principles presented in the following section.

3.3. Existence of C–S–H/epoxy nanocomposite

Neat C–S–H can be modeled using a polycrystalline self-consistent micromechanics model that assumes spherical morphology of the C–S–H solid [25,36 to estimate the effective elastic modulus of C–S–H phases. Self-consistent relationship between reduced modulus and packing density of C–S–H, per Constantinides and Ulm [25], is given by a dashed line in Fig. 13 with data points for LD and HD C–S–H from this study, where packing density is defined per eq. (1).

The lower bound on the packing density of 0.50 represents a minimum percolation threshold and is approximately equal to the random loose-packed limit of spheres of 0.56 [37]. Values of packing density lower than 0.50 are not physically admissible for spherical inhomogeneity geometry. The packing density of 1.0 assumes C–S–H solid with a reduced modulus of 65 GPa occupies the entire REV, as

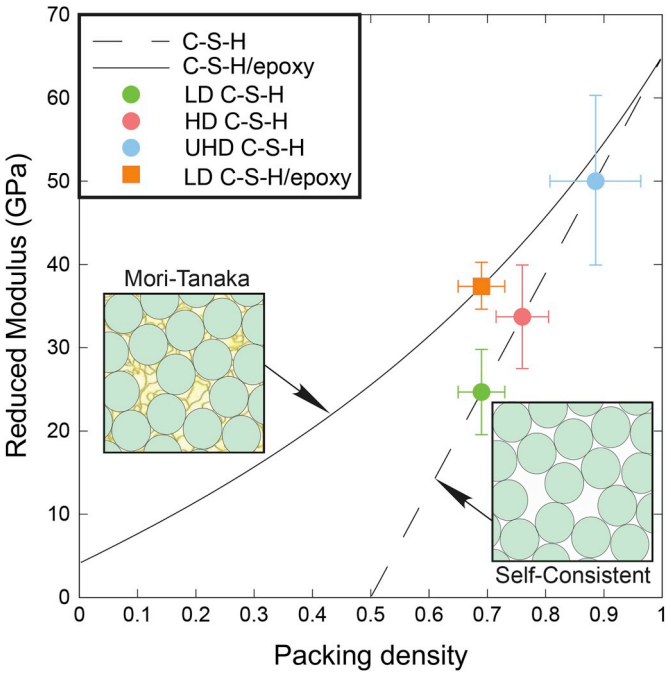

Fig. 13. Reduced moduli of C–S–H and C–S–H/epoxy composite based on self-consistent and Mori-Tanaka micromechanical schemes.

determined by Pellenq et al. [11].

At the length scale of Level I, the amount of gel porosity in neat C–S–H (defined by packing density—eq. (1)) is a function of multiple variables (degree of hydration, cement composition, cement particle size distribution, etc.). Packing density ranges, based on an extensive nanoindentation experimental program by Vandamme [32], are listed in Table 2. Based on the reduced modulus-packing density relationship established by self-consistent micromechanics formulation (Fig. 13), LD C–S–H, HD C–S–H, and UHD C–S–H of the studied cement paste were found to have the average packing densities of 0.68, 0.76, and 0.89, respectively. The three values are well within the range of packing densities reported in the literature (Table 4). The packing density of LD C–S–H is close to the theoretical random packing limit of equal spheres

(0.64). The density of ordered (face-centered cubic) packing of equal spheres ($\pi/3\sqrt{2} = 0.74$) is close to that of HD C–S–H [38]. The mean packing density of UHD C–S–H of 0.89 is significantly greater than the maximum packing density of equal spheres which indicates that UHD C–S–H would have to consist of multi-sized spheres. A theoretical upper limit on the packing density of two-sized spheres is $1 - (1 - \pi/3\sqrt{2})^2 = 0.93$ which is close to a computed packing density of 0.89 [39]. The assumption of two-sized sphere morphology is in agreement with the finding that UHD C–S–H represents a nanocomposite consisting of two phases – HD C–S–H and CH nanocrystals [20].

When epoxy fills the pore space within LD C–S–H, it can be regarded as a matrix phase with the C–S–H globules representing inhomogeneities within the matrix. In this configuration, Mori-Tanaka micromechanical model is a more suitable choice for estimation of the effective modulus [40]. Even at high concentrations of isotropic spherical inclusions, which would be typical for the range of packing densities associated with LD C–S–H, Mori-Tanaka homogenization scheme was proven to be valid [41]. Mori-Tanaka method also overcomes the inaccuracies associated with self-consistent model for matrix-inclusion morphology when inhomogeneities are relatively rigid compared to the matrix phase [42]. By assuming spherical morphology of C–S–H globules, effective reduced modulus of C–S–H/epoxy composite per Mori-Tanaka homogenization scheme was plotted with a solid line in Fig. 13 for a range of packing densities. Material properties used in the model are summarized in Table 7. For the employed matrix-inclusion morphology, the packing density represents a relative volumetric ratio of C–S–H solid and epoxy matrix within the REV. Per Mori-Tanaka micromechanical model, the composite of LD C–S–H and epoxy has an effective reduced modulus of 37.4 ± 2.5 GPa for a packing density in the 0.69 ± 0.03 range (Fig. 13), which is significantly greater than the reduced modulus of HD C–S–H of 33.2 ± 6.2 GPa. The micromechanics evaluation of C–S–H/epoxy composite, thus, explains the increase in average reduced modulus of HD Phase of in the interphase region at 55 μm and 77.5 μm away from the interface.

The results of the herein presented micromechanical analysis are also in agreement with the postulated composition of HD Phase in the interphase region. Obtained effective modulus of LD C–S–H and epoxy composite, per Mori-Tanaka method, provides an adequate explanation for the changing ratio of LD Phase to HD Phase with respect to distance from the interface. Continuum micromechanics analysis also confirmed the important effect of cement paste porosity on mechanical properties within the interphase region: based on the results, it can be expected that interphase properties could widely vary between substrates of dissimilar porosity. Effective reduced modulus estimate of LD C–S–H/epoxy composite, based on Mori-Tanaka method, represents the upper bound on the effective reduced modulus value for C–S–H/epoxy composite since the analytical procedure assumes that all porosity within C–S–H is filled with epoxy. In a real-world scenario, the gel porosity would be partially or completely filled with moisture which would likely significantly affect the permeation of epoxy into the porous structure of LD C–S–H. Further work is required to provide a better understanding of moisture effects and porous network interconnectivity on the epoxy-cement paste adhesive interphase properties.

4. Summary and conclusions

Previous work on epoxy-cement paste interactions within the interface region were used to develop the elastic multiscale continuum model for epoxy-cement paste interphase proposed in this paper. Nanoindentation experiments were conducted to provide experimental evidence in support of the proposed model.

Site-specific statistical nanoindentation in the interphase region between cement paste and epoxy was conducted and four mechanically distinct material phases were identified in the interphase region: LD Phase, HD Phase, UHD Phase, and clinker. Based on the experimental results, LD and HD Phase experienced degradation of reduced modulus and hardness adjacent to the interface due to the dissolution effect of epoxy hardener on cement paste hydration products [17]. Stiffening of cement paste within the interphase region occurred at 55 and 77.5 μm away from the interface, and reflected mainly in the increase of the reduced modulus of HD Phase. Analysis of volume fractions of the interphase material phases showed a gradual increase in the volume fraction of LD Phase on the account of HD Phase. Continuum micromechanics models were used to show that this behavior is due to the formation of LD C–S–H and epoxy nanocomposite. Mori-Tanaka homogenization scheme explained the observed change in volume fractions with distance from the interface—epoxy permeation into the cement paste pores was found to lead to an increase in the effective reduced modulus of LD C–S–H by as much as 50%.

Table 7
Summary of material properties used in micromechanical models.

Material	Reduced Modulus	Poisson's Ratio
Epoxy	4.40 GPa[a]	0.40 [34]
C–S–H Solid	65 GPa [11]	0.30 [11]

[a] Based on nanoindentation experiments.

Acknowledgements

The authors gratefully acknowledge the financial support provided by Byron D. Spangler Professorship at the University of Florida, and internal funds at the University of Delaware.

References

[1] Mays GC, Hutchinson GC. Adhesives in civil engineering. Cambridge, United Kingdom: Cambridge University Press; 1992.
[2] Petrie HM. Handbook of adhesives and sealants. New York, NY: McGraw-Hill Professional Publishing; 2006.
[3] Tatar J, Subhash G, Taylor CR, Hamilton HR. Characterization of adhesive interphase between epoxy and cement paste via Raman spectroscopy and mercury intrusion porosimetry. Cement Concr Compos 2018;88:187–99.
[4] Djouani F, Connan C, Delamar M, Chehimi MM, Benzarti K. Cement paste-epoxy adhesive interactions. Constr Build Mater 2011;25:411–23.
[5] Stewart A, Scholsser B, Douglas EP. Surface modification of cured cement pastes by silane coupling agents. J Appl Mater Interfaces 2013;5(4):1218–25.
[6] Sharpe LH. "Interfaces, interphases and "adhesion": a perspective.". In: Akovali G, editor. The. Interfacial interactions in polymeric composites. NATO ASI series (series E: applied sciences, vol 230. Dordrecht: Springer; 1993.
[7] Zanni-deffarges MP, Shanahan MER. Bulk and interphase effects in aged structural joints. J Adhes 1994;45(1–4):245–57.
[8] Ulm FJ, Delafargue A, Constantinides G. Experimental microporomechanics. In: Dormieux L, Ulm FJ, editors. Applied micromechanics of porous materials. Dordrecht: Springer; 2005. p. 207–88.
[9] Tatar J, Torrence C, Mecholsky JJ, Taylor CR, Hamilton HR. Effects of silane surface functionalization on interfacial fracture energy and durability of adhesive bond between cement paste and epoxy". Int J Adhesiv Adhes 2018;84:132–42.
[10] Richardson IG, Groves GW. Microstructure and microanalysis of hardened cement pastes involving ground granulated blast-furnace slag. J Mater Sci 1992;27(22):6204–12.
[11] Pellenq RJM, Kushima A, Shahsavari R, Van Vliet KJ, Buehler MJ, Yip S, Ulm FJ. A realistic molecular model of cement hydrates. Proc Natl Acad Sci Unit States Am 2009;106(38):16102–7.
[12] Qomi MJA, Krakowiak KJ, Bauchy M, Stewart KL, Shahsavari R, Jagannathan D, Brommer DB, Baronnet A, Buehler MJ, Yip S, Ulm FJ, Van Vliet KJ, Pellenq RJM. Combinatorial molecular optimization of cement hydrates. Nat Commun 2014;5.
[13] Ulm F-J, Constantinides G, Heukamp FH. "Is concrete a poromechanics material? – a multiscale investigation of poroelastic properties". Mater Struct 2004;37(1):43–58.
[14] Feldman RF, Sereda PJ. A model for hydrated Portland cement paste as deduced from sorption-length change and mechanical properties. Mater Struct 1968;1(6):509–20.
[15] Powers TC, Brownyard TL. Studies of the physical properties of hardened Portland cement paste. PCA Bull 1948;22.
[16] Jennings HM. A model for the microstructure of calcium silicate hydrate in cement paste. Cement Concr Res 2000;30(1):101–16.
[17] Djouani F, Chehimi MM, Benzarti K. Interactions of fully formulated epoxy with model cement hydrates. J Adhes Sci Technol 2013;27(5–6):469–89.
[18] Viallis-Terrisse H. "Interaction des Silicates de Calcium Hydratés, principaux constituants du ciment, avec les chlorures d'alcalins. Analogie avec les argiles. Université de Bourgogne; 2000 [PhD Thesis]. [France].

[19] Pelisser F, Gleize PJP, Mikowski A. Effect of the Ca/Si molar ratio on the micro/nanomecanical properties of syntetic C-S-H measured by nanoindentation. J Phys Chem C 2012;116:17219–27.
[20] Chen J, Sorelli L, Vandamme M, Ulm FJ, Chavillard G. A coupled nanoindentation/SEM-EDS study on low water/cement ratio Portland cement paste: evidenve for C-S-H/Ca(OH)2 nanocomposites. J Am Ceram Soc 2010;93(5):1484–93. Wiley.
[21] Constantinides G, Ulm F-J. The effect of two types of C-S-H on the elasticity of cement-based materials: results from nanoindentation and micromechanical modeling. Cement Concr Res 2004;34(1):67–80.
[22] Davydov D, Jirasek M, Kopecky L. Critical aspects of nano-indentation technique in application to hardened cement paste. Cement Concr Res 2011;41(1):20–9.
[23] Nemecek J. Nanoindentation based analysis of heterogeneous structural materials. In: Nemecek Jiri, editor. Chapter in nanoindentation in materials science; 2012.
[24] Randall NX, Vandamme M, Ulm F-J. Nanoindentation analysis as a two-dimensional tool for mapping the mechanical properties of complex surfaces. J Mater Res 2009;24(3):679–90.
[25] Constantidines G, Ulm FJ. The nanogranular nature of C-S-H. J Mech Phys Solids 2007;55(1):64–90.
[26] Oliver WC, Pharr GM. An improved technique for determining hardness and elastic modulus using load and displacement sensing indentation experiments. J Mater Res 1992;7(6):1564–83.
[27] Krakowiak KJ, Wison W, James S, Musso S, Ulm FJ. Inference of the phase-to-mechanical property link via couples X-ray spectrometry and indentation analysis: application to cement-based materials. Cement Concr Res 2015;67:271–85.
[28] Schwartz GE. Estimating the dimension of a model. Ann Stat 1978;6(2):461–4.
[29] Mitchell LD, Margeson JC. The effects of solvents on C-S-H as determined by thermal analysis. J Therm Anal Calorim 2006;86(3):591–4.
[30] Burton B, Alexander D, Klein H, Garibay-Vasquez A, Pekarik A, Henkee C. Epoxy formulations using Jeffamine® polyetheramines. Huntsman Corporation; 2005.
[31] Trtik P, Dual J, Muench B, Holzer L. "Limitations in obtainable surface roughness of hardened cement paste: 'virtual' topographic experiment based on focused ion beam nanotomography datasets". J Microsc 2008;232(2):200–6.
[32] Vandamme M. The nanogranular origin of concrete creep: a nanoindentation investigation of microstructure and fundamental properties of calcium-silicate-hydrate. Ph.D. Dissertation. Cambridge, MA: Massachusetts Institute of Technology (MIT); 2008.
[33] Vanzo J. A nanochemomechanical investigation of carbonated cement paste. M.S. Thesis. Cambridge, MA: Massachusetts Institute of Technology (MIT); 2009.
[34] Hollmann K, Hahn HT. Acoustic emission behavior of epoxies during tensile loading. Polym Eng Sci 1989;29(8):513–22.
[36] Hill R. A self-consistent mechanics of composite materials. J Mech Phys Solids 1965;13:213–22.
[37] Jaeger HM, Nagel SR. Physics of the granular state. Science 1992;255(5051):1523–31.
[38] Hales Thomas C. A proof of the Kepler conjecture. Ann Math, Second Ser 2005;162(3):1065–185.
[39] Yamada S, Kanno J, Miyauchi M. Multi-sized sphere packing in containers: optimization formula for obtaining the highest packing density with two different sized spheres. IPSH Online Trans 2011;4:126–33.
[40] Mori T, Tanaka K. Average stress in the matrix and average elastic energy of materials with misfitting inclusions. Acta Metall 1973;21:571–4.
[41] Ferrari M. Asymmetry and the high concentration limit of the Mori-Tanaka effective medium theory. Mech Mater 1991;11:251–6.
[42] Qu J, Cherkaoui M. Fundamentals of micromechanics of solids. Hoboken, New Jersey: John Wiley & Sons, Inc.; 2006.
[35] ASTM D638. Standard test method for tensile properties of plastics. West Conhohocken, PA: ASTM International; 2014. 2014.